Test–retest of a phoria adaptation stimulus-induced functional MRI experiment

Cristian Morales　　Biomedical Engineering, New Jersey Institute of Technology, Newark, NJ, USA　✉

Suril Gohel　　Department of Health Informatics, Rutgers University School of Health Professions, Newark, NJ, USA　✉

Mitchell Scheiman　　Pennsylvania College of Optometry, Salus University, Philadelphia, PA, USA　✉

Xiaobo Li　　Biomedical Engineering, New Jersey Institute of Technology, Newark, NJ, USA　✉

Elio M. Santos　　Biomedical Engineering, New Jersey Institute of Technology, Newark, NJ, USA　✉

Ayushi Sangoi　　Biomedical Engineering, New Jersey Institute of Technology, Newark, NJ, USA　✉

Tara L Alvarez　　Biomedical Engineering, New Jersey Institute of Technology, Newark, NJ, USA　✉

This study was designed to identify the neural substrates activated during a phoria adaptation task using functional magnetic resonance imaging (MRI) in young adults with normal binocular vision and to test the repeatability of the fMRI measurements for this protocol. The phoria adaptation task consisted of a block protocol of 90 seconds of near visual crossed fixation followed by 90 seconds of far visual uncrossed fixation, repeated three times; the data were collected during two different experimental sessions. Results showed that the oculomotor vermis, cuneus, and primary visual cortex had the greatest functional activity within the regions of interest studied when stimulated by the phoria adaptation task. The oculomotor vermis functional activity had an intraclass correlation coefficient (ICC) of 0.3, whereas the bilateral cuneus and primary visual cortex had good ICC results of greater than 0.6. These results suggest that the sustained visual fixation task described within this study reliably activates the neural substrates of phoria adaptation. This protocol establishes a methodology that can be used in future longitudinal studies investigating therapeutic interventions that may modify phoria adaptation.

Introduction

Phoria adaptation refers to a phenomenon that occurs when a person performs a sustained visual task that creates stress on the accommodative/convergence system. Phoria adaptation reduces the effort exerted by the disparity vergence system to maintain fusion. Binocular vision dysfunctions such as convergence insufficiency are generally defined by an abnormal relationship between the magnitude of the phoria and the compensating fusional vergence (Scheiman & Wick, 2020). In addition, abnormal phoria adaptation has been suggested as a potential contributing factor to binocular dysfunctions such as convergence insufficiency (Brautaset & Jennings, 2005a; Brautaset & Jennings, 2005b; Schor & Horner, 1989). Numerous studies have investigated how the phoria level changes throughout the day (Henson & North, 1980; Judge, 1996). After near sustained fixation, such as while reading or working on electronic devices, the phoria becomes more esophoric. Conversely, after distance viewing, the phoria becomes more exophoric. Researchers have developed several paradigms to

evaluate phoria adaptation. The phoria can be adapted using sustained visual fixation (Han, Guo, Granger-Donetti, Vicci, & Alvarez, 2010; Kim, Vicci, Granger-Donetti, & Alvarez, 2011; Kim, Vicci, Han, & Alvarez, 2011; Lee, Granger-Donetti, Chang, & Alvarez, 2009), visual stimulation through the use of prisms (Brautaset & Jennings, 2005a; Brautaset & Jennings, 2005b; Schor, 1988), or visual stimulation through the use of lenses (Jiang, Tea, & O'Donnell, 2007; Sreenivasan, Irving, & Bobier, 2008; Sreenivasan, Irving, & Bobier, 2009).

Several areas of research suggest that the cerebellar cortex is one neural substrate that mediates phoria adaptation and oculomotor learning (Bostan & Strick, 2018; Raymond & Medina, 2018), as well as procedural learning (Molinari, Leggio, Solida, Ciorra, Misciagna, Silveri, & Petrosini, 1997). Animal studies in rabbits, cats, and primates support the idea that the oculomotor vermis, which is comprised of the cerebellar vermal regions VI and VII, is partially responsible for the mediation of phoria adaptation (Milder & Reinecke, 1983; Takagi, Tamargo, & Zee, 2003). Researchers report that patients with cerebellar atrophy and dysfunction exhibit little or no phoria adaptation while using prisms (Milder & Reinecke, 1983; Robertson & Miall, 1999). Numerous studies support the suggestion that cerebellar dysfunctions are commonly observed in developmental dyslexia (Eckert, Leonard, Richards, Aylward, Thomson, & Berninger, 2003; Nicolson, Fawcett, & Dean, 2001; Stoodley, Fawcett, Nicolson, & Stein, 2005; Vicari, Finzi, Menghini, Marotta, Baldi, & Petrosini, 2005; Vicari, Marotta, Menghini, Molinari, & Petrosini, 2003). Several investigations have reported dyslexic readers with deficits in vergence and other oculomotor function (Bucci, Brémond-Gignac, & Kapoula, 2008; Bucci, Nassibi, Gérard, Bui-Quoc, & Seassau, 2012; Kapoula & Bucci, 2007; Legrand, Bui-Quoc, Doré-Mazars, Lemoine, Gérard, & Bucci, 2012; Przekoracka-Krawczyk, Brenk-Krakowska, Nawrot, Rusiak, & Naskręcki, 2017). In addition, studies on strabismic patients also suggest dysfunction in the cerebellum (Gaertner, Creux, Espinasse-Berrod, Orssaud, Dufier, & Kapoula, 2013; Przekoracka-Krawczyk, Nawrot, Kopyciuk, & Naskręcki, 2015). Collectively, these lines of research indicate that the cerebellum is part of the neural circuit needed to mediate vergence eye movement function. Functional magnetic resonance imaging (fMRI) is a research tool that could be used to determine the neural substrates of phoria adaptation in normal control participants. A functional MRI investigation studying the impact of the accuracy of finger pointing when viewed through a prism reported that the dentate nucleus and cerebellar cortex, specifically the vermis, are significantly active during the early stage of motor learning (Küper et al., 2014). A recent review paper observed that the cerebellum has a major role in motor learning and error

correction (Bostan & Strick, 2018), but its role within phoria adaptation is not completely understood.

A present gap in the literature is an understanding of the full neural circuit used to mediate phoria adaptation. This understanding is important because phoria adaptation has been shown to differ significantly between those with normal binocular vision and those with impairments in binocular vision, such as patients with convergence insufficiency (Brautaset & Jennings, 2005b; North & Henson, 1981). Such knowledge may lead to novel methods that target specific neural circuits to improve visual function in patients with binocular dysfunction who have been shown to have reduced phoria adaptation compared to age-matched control participants. In addition, if phoria adaptation is to be used as an outcome measure for future randomized clinical trials, then it is important to determine the reliability of any assessment protocol used to investigate phoria adaptation.

Currently, a gap in the literature is the lack of reliable information about the regions of interest (ROIs) that are recruited during a sustained visual task known to evoke phoria adaptation. In addition, the reliability of fMRI assessment during a phoria adaptation task measured on different days is unknown. Quantifying the reliability of an fMRI experimental protocol is critical if phoria adaptation is to be used as an outcome measure for future randomized clinical trials. The research goals of this study of healthy young adults with normal binocular vision were to establish which ROIs are functionally active during a phoria adaptation task that utilizes sustained visual fixation and to assess the reliability of a stimulus-induced phoria adaptation task during a functional MRI experiment. The study tested the hypothesis that phoria adaptation will stimulate functional activity within the vergence network, where the primary functional activation is proposed to reside within the cerebellar oculomotor vermis.

Methods

Participants

A total of 29 young adult participants with normal binocular vision who were between the ages of 18 and 35 years (21.7 ± 3.3 years; five females) were studied. All participants signed written informed consent approved by the New Jersey Institute of Technology and the Rutgers University Institutional Review Boards in accordance with the tenets of the Declaration of Helsinki. All potential participants had a comprehensive eye examination to determine study eligibility. To be eligible for the normal binocular vision group, participants were assessed by an optometrist (one of the authors, MS) and met the eligibility and exclusion criteria described in Table 1.

Normal binocular vision eligibility criteria
Age 18 to 35 years
Convergence Insufficiency Symptom Survey score < 21
Distance phoria: 2Δ esophoria to 4Δ exophoria
Near phoria: 2Δ esophoria to 6Δ exophoria
Normal near point of convergence of <6 cm break
Normal positive fusional vergence (PFV) at near (i.e., passing Sheard's criterion or PFV $\geq 15\Delta$ base-out break)
Normal amplitude of accommodation (minimum of $15\text{-}1/4 \times$ age)
Best-corrected distance visual acuity of 20/25 or better in each eye
Local random dot stereopsis appreciation of 70 seconds of arc or better
Did not use a biprism or plus add lens at near for 2 weeks prior to study

Normal binocular vision exclusion criteria
Strabismus
Vertical heterophoria $\geq 2\Delta$ at distance or near
≥ 2 line interocular difference in best-corrected visual acuity
Manifest or latent nystagmus
History of strabismus surgery or refractive surgery
History of head trauma or known disease of the brain
History of diseases known to affect accommodation, vergence, or ocular motility
Inability to comprehend and/or perform any study-related test

Table 1. Eligibility criteria for normal binocular vision (NBV).

Eligibility eye examination

The eligibility eye examination included administration of the Convergence Insufficiency Symptom Survey (CISS) to identify whether or not the participant was symptomatic (Borsting et al., 2003; CITT-ART Investigator Group et al., 2015). Other eligibility tests included best-corrected visual acuity at distance and near; a sensorimotor examination that included a cover test at distance and near, near point of convergence, positive and negative fusional vergence at near (prism bar and a held 20/30 vertical line of letters as a target), vergence facility (12Δ base-out, 3Δ base-in prism) at distance and near, and near stereoacuity (Randot Stereotest); and monocular accommodative amplitude (20/30 target) using a Gulden Near Point Rule (Gulden Ophthalmics, Elkins Park, PA). Full details are described in a prior publication (Alvarez et al., 2020).

Experimental setup to acquire functional brain images

Anatomical and functional brain images were acquired using a Siemens 3T Trio scanner (Siemens Medical Solutions, Parkway Malvern, PA) located in the Rutgers University Brain Imaging Center of Rutgers University (Newark, NJ). A 12-channel head coil was used for all of the participants to scan a full brain volume. A schematic of the equipment used during the experiment is shown in Figure 1A. Monocular eye position was acquired using an EyeLink 1000 system (SR Research, Kanata, ON, Canada) with a sampling rate of 250 Hz to ensure that the participants performed the visual tasks as instructed (Guo, Kim, & Alvarez, 2011). Binocular visual position was not available during these scanning sessions because the instrument for binocular recording obstructed visual sight for other experiments. The participants were aligned symmetrically on the gantry within the bore of the magnet. Within the head coil was an inclined mirror facing the posterior end of the bore of the magnet.

A projector was placed in the back of the room so that the participant could view the visual stimuli through a mirror located on the headcoil. The distance between the screen and the participant's eyes was 87.5 cm. The screen dimensions were 36 cm for the width and 20.5 cm for the height. The screen was configured at 1920×1080-pixel resolution and a 60-Hz refresh rate. Visual stimuli were generated and presented using MATLAB (MathWorks, Natick, MA) and Psychtoolbox (Brainard, 1997) on a personal computer located in the MRI control room.

Eye position on the EyeLink was calibrated at the beginning of the scan by asking the participant to move his or her eyes toward five predetermined positions established by the manufacturer: upper left and right, center, and lower left and right portions of the liquid-crystal display screen. Such calibration allowed the conversion to angular rotation of the eye in degrees.
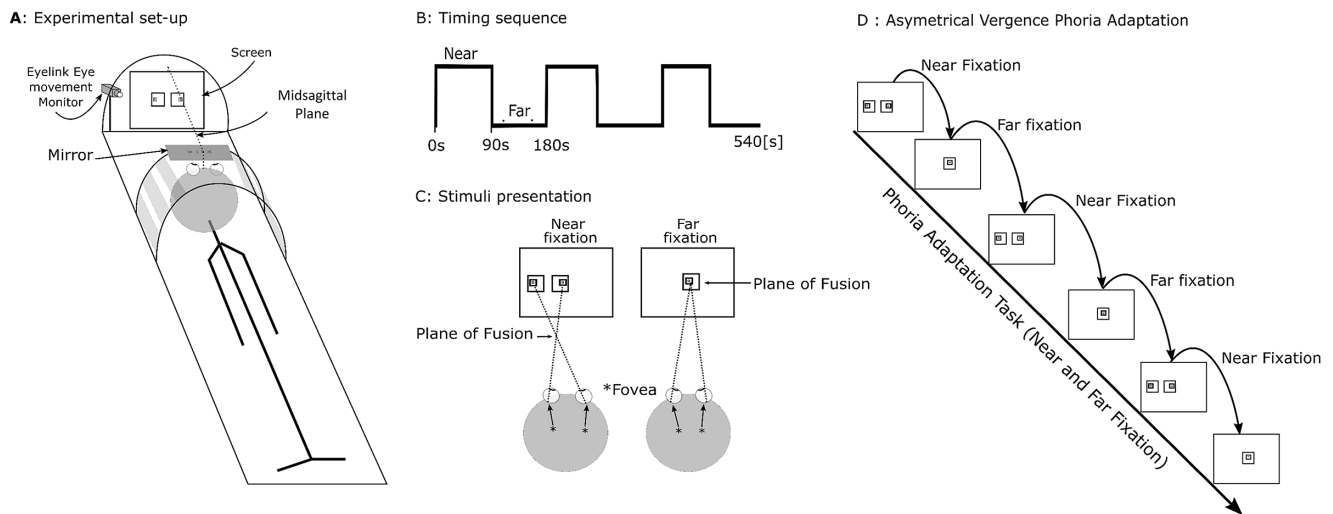
Figure 1. (A) Experimental setup within the MRI scanner room. The participant lies on the gantry within the bore of the magnet and observes the screen through a mirror placed along the top of the head coil. (B) Timing sequence of the phoria adaptation task. The stimuli began with a near crossed sustained convergence visual stimulus for 90 seconds followed by a far uncrossed sustained visual stimulus for 90 seconds, a process that was repeated three times for a total of 540 seconds. (C) Visual stimulus presentation for the near crossed and far uncrossed sustained fixation task. (D) Visual stimulus timing sequence that alternates between near crossed and far uncrossed visual sustained fixation.

Behavioral phoria adaptation experiments within the laboratory

Phoria adaptation was measured prior to the scanning session in the laboratory using the modified Thorington method utilizing the Bernell Muscle Imbalance Measure (MIM) card and Maddox rod (Bernell Corp., Mishawaka, IN). Phoria adaptation measures were recorded in the morning prior to any substantial near work. To establish a baseline, the phoria was measured twice using the flashed modified Thorington/Maddox rod technique (Han et al., 2010). Specifically, the left eye was occluded for 15 seconds while the Maddox rod was placed in front of the right eye. When the occluder was removed, the participant was asked to verbally specify the location of the vertical red streak on the MIM card while fixating on the central pen light located along the midsagittal plane 40 cm away. Each participant then performed sustained fixation on a 20/30 letter chart placed immediately above the MIM card when looking through a 6Δ base-in prism for 30 seconds. The participant's phoria level was then measured once after every 30 seconds of binocular viewing of the 20/30 letter chart through the prism using the same technique described above. Fifteen samples were recorded during the 7-minute experiment for each participant.

Placing a prism in front of one eye stimulates asymmetrical phoria adaptation, as opposed to symmetrical phoria adaptation, which occurs when the prism is equally split between the two eyes (prism flipper). Asymmetrical phoria adaptation has been shown to lead to a faster rate of change compared to symmetrical phoria adaptation (Santos, Yaramothu, & Alvarez, 2018). Hence, an asymmetrical prism adaptation procedure was used in this study. After the 6 base-in phoria adaptation experiment, participants then took a 15-minute break and were instructed to relax their eyes and walk in the hallway after the experiment. After the 15-minute break, two baseline phoria measurements were recorded to determine whether the phoria returned to the original baseline measurements. The phoria adaptation experiment was then repeated using a 6Δ base-out prism. The complete procedure is described in a previous publication (Alvarez et al., 2020; Santos et al., 2018).

The behavioral phoria adaptation results, recorded outside of the scanner, were fit with an exponential function. The two primary metrics analyzed were the magnitude and the rate of phoria adaptation. The magnitude of phoria adaptation was the difference between the initial shift in phoria and the steady state of the adapted phoria. The rate of phoria adaptation was defined as the magnitude of the phoria adaptation divided by the time constant from the exponential fit of the data.

Phoria adaptation stimuli for fMRI experiment

To stimulate phoria adaptation for the functional MRI experiment, sustained fixation was utilized.

This method of testing phoria adaptation has been shown to be an effective method ([Alvarez, Kim, & Granger-Donetti, 2017](); [Chen, Lee, Chen, Semmlow et al., 2010](); [Kim, Granger-Donetti, Vicci, & Alvarez, 2010](); [Kim, Vicci, Granger-Donetti, & Alvarez, 2011](); [Kim, Vicci, Han, & Alvarez, 2011](); [Lee et al., 2009]()) and does not require any physically moving parts. The overall timing sequence is shown in [Figure 1]()B. The visual stimulus was a set of eccentric squares ([Figure 1]()C) that stimulate a perception of an object being close to the participant (near visual sustained crossed disparity) or farther from the participant (far visual sustained uncrossed disparity). Prior to the functional imaging experiment, the participants were asked to perform free fusion in the laboratory, where they practiced crossing and uncrossing their gaze. When the participant was able to report the inner eccentric square as floating in front or behind the outer square then the experimenter was confident that the participant was able to perform the visual task. The outer square subtended a vergence angle of 2° by 2°. Our research group has shown that an asymmetrical 6Δ phoria adaptation task has a faster time constant compared to a symmetrical 6Δ phoria adaptation task ([Santos et al., 2018]()). Hence, phoria adaptation was stimulated asymmetrically analogous to the presentation for the behavioral experiments.

A single square centered in the middle of the screen was presented to induce the perception of distance (far uncrossed disparity) for far phoria adaptation. The change in retinal disparity between the near and far visual fixations was analogous to the behavior experiments of 6Δ. The mirror was carefully positioned so that the participant did not observe the edge of the projector screen. The set of two eccentric squares was presented to stimulate near crossed phoria adaptation. The phoria adaptation visual sequence consisted of sustained fixation for 90 second durations each repeated for 6 blocks. Because phoria adaptation follows an exponential decay, the greatest change occurs within the beginning portion of the phoria adaptation. The 90-second duration for each block was chosen because the behavioral data showed that the greatest change in phoria occurred within the first 90 seconds of the 7-minute phoria adaptation experiment measured within the lab. Other investigations that have stimulated phoria adaptation for several minutes support the suggestion that the largest change in phoria occurs within the first 90 seconds ([Brautaset & Jennings, 2005b](); [Henson & North, 1980]()). A total of 270 volumes were collected for the phoria adaptation experiment within the imaging center. The full timing sequence is detailed in [Figure 1]()D. The task began with a near crossed sustained visual fixation block followed by a far uncrossed visual fixation block, and this sequence was repeated three times.

Scanning protocol

Imaging data were acquired from participants on two different days. The same acquisition protocol was performed on each visit. During the visit, an anatomical high-resolution image was acquired using a magnetization-prepared rapid acquisition gradient echo (MP-RAGE) sequence as a reference volume (repetition time [TR] = 1900 ms; 176 slices; echo time [TE] = 2.52 ms; inversion time [TI] = 900 ms; flip angle = 9°; field of view [FOV] = 256 mm; voxel size = 1 mm^3). The fMRI acquisition used an echo planar imaging (EPI) sequence (TR = 2000 ms; TE = 13 ms; flip angle = 90°; FOV = 192 mm; voxel size = 3 mm^3; 53 slices; total of 270 volumes). Simultaneously, with the fMRI data acquisition, the functional sustained visual task used to stimulate phoria adaptation was presented during the 540 seconds.

Image preprocessing

The EPI functional image dataset from each visit was analyzed using SPM 12 for MATLAB (Wellcome Centre for Human Neuroimaging, London, UK), using the default parameters. The following preprocessing was performed for each EPI functional image dataset independently. All of the volumes within the acquisition were realigned to the first volume. The realignment procedure returns the head motion for the following six directions: *x*, *y*, and *z* movements within a slice, as well as pitch, yaw, and roll movements between slices. Datasets with more than 2 mm of motion between time samples were not further analyzed. The realigned volumes were co-registered to each participant's MP-RAGE anatomical dataset.

Following co-registration, each of the MP-RAGE anatomical image datasets was segmented into tissue-probability maps representing white matter (WM) and cerebrospinal fluid (CSF). Binary masks for both WM and CSF were generated from tissue-probability maps using the threshold equal to 97% or greater. These binary masks were used to extract the blood-oxygen-level-dependent (BOLD) fMRI time series from the CSF and WM regions for each participant. Principal component analysis was implemented to extract the five principal components representing CSF and the five principal components representing WM time series using a custom MATLAB function ([Behzadi, Restom, Liau, & Liu, 2007]()).

The BOLD fMRI data for each participant were transformed to the Montreal Neurological Institute (MNI152) template, and the functional volume were resampled to a 2-mm isotropic voxel-size using a fourth-degree b-spline interpolation within the SPM12 Normalize function. In order to reduce the effects of

movement-related and physiological noise artifacts on task activation, 34 nuisance variables were regressed out from the BOLD fMRI data within the MNI standard space. These nuisance variables were comprised of six movement coefficients (yaw, pitch, roll, *x*, *y*, and *z*), six auto-regression and 12 quadratics (Friston, Williams, Howard, Frackowiak, & Turner, 1996; Yan et al., 2013), first five principal components of the CSF, and the first five principal components of the WM (using CompCorr) (Behzadi et al., 2007; Servatius, Spiegler, Handy, Pang, Tsao, & Mazzola, 2018). The resulting functional volume datasets were high-pass filtered with a cutoff frequency (f_c) equal to 1/256 Hz, or 0.0039 Hz. Each volume was then spatially smoothed with a Gaussian kernel of 6 mm full width at half maximum.

Whole-brain activation map and group level statistics

A general linear model (GLM)-based approach (Monti, 2011) was implemented to derive participant-specific task-based activation maps for the phoria-adaptation task. The task design was composed of 90 seconds of near crossed visual fixation followed by 90 seconds of far uncrossed visual fixation block repeated three times (Figure 1B). Behavioral studies show that the phoria response exhibits an exponential decay; thus, for the GLM, a delta block of 4 seconds combined with the exponential decay obtained from the behavioral phoria adaptation experiment was utilized. The delta block was convolved with a canonical hemodynamical response function, the double-gamma hemodynamic response function. The functional imaging beta weights were calculated for the delta response using the GLM for each participant. This process was also used to derive the participant-specific functional activation maps for the phoria adaptation task for visit 2. For each of the two visits, group-level activation maps were derived using a one-sample *t*-test. For the group-level analyses, the datasets were corrected for multiple comparisons using whole-brain clusterwise family wise error (FWE) with a threshold of $p < 0.05$ (Flandin & Friston, 2019).

Selection of regions of interest

In addition to determining test–retest reliability of the phoria adaptation task, one goal of this study was to identify the ROIs during a phoria adaptation task to develop masks for future research. To this end, based on previous studies on vergence eye movements, the following neural substrates were identified as regions of interests: frontal eye fields (FEFs), parietal eye fields (PEFs), supplementary eye field (SEF), bilateral cuneus, cerebellar vermis, and the primary visual cortex

(Alvarez, Alkan, Gohel, Douglas Ward, & Biswal, 2010; Alvarez, Jaswal, Gohel, & Biswal, 2014; Alvarez et al., 2010; Jaswal, Gohel, Biswal, & Alvarez, 2014; Morales et al., 2020). Initially, an ROI mask composed of a 5-mm sphere was created, based on the MNI coordinates identified in our earlier study (Morales et al., 2020). Then, the ROI mask was optimized by selecting the center coordinate as the pixel with the peak intraclass correlation coefficient (ICC) (see following section) value within each ROI and creating a 5-mm sphere around the pixel with the peak ICC. The ROIs were generated using MarsBaR for SPM and MATLAB (Brett, Anton, Valabregue, & Poline, 2002).

Reliability evaluation

Assessment of magnitude of functional activity

The intraclass correlation coefficient is an index designed to measure reliability. There are six variants of ICC dependent on the number of examiners and the number of samples acquired (Shrout & Fleiss, 1979). In the current study, one stimuli paradigm in one population group using one experimental setup and the same facility in visits on different days was examined. The ICC used to assess the repeatability of functional activity is described within Equation 1:

$$ICC\,(1,1) = \frac{MS_B - MS_W}{MS_B + (k-1)\,MS_W} \quad (1)$$

where MS_B is the mean squared beta weight between participants, MS_W is the mean squared beta weight within an individual participant, and *k* is the number of participants. Test–retest reliability is classified as poor (ICC = 0 to 0.4), fair (ICC = 0.4 to 0.55), good (ICC = 0.55 to 0.75), or excellent (ICC = 0.75 to 1.0) (Gorgolewski, Storkey, Bastin, Whittle, & Pernet, 2013; Li, Zeng, Lin, Cazzell, & Liu, 2015; Lukasova et al., 2014; Morrison, Das, Graham, Cusimano, Schweizer, & Churchill, 2016). The ICC values were calculated using the IPN toolbox to assess reliability in MATLAB (Zuo, Di, et al., 2010; Zuo, Kelly, Adelstein, Klein, Castellanos, & Milham, 2010).

Assessment of spatial extent reliability

Prior research cautions that spatial extent measurements are very sensitive to motion artifacts (Gorgolewski et al., 2013). Hence, a more stringent exclusion criterion for data inclusion was utilized. Specifically, only participants who had less than 1 mm mean movement across each session were included in the group-level analysis of the reliability of spatial extent. To assess the repeatability of spatial extent, the group-level activation maps were generated for a
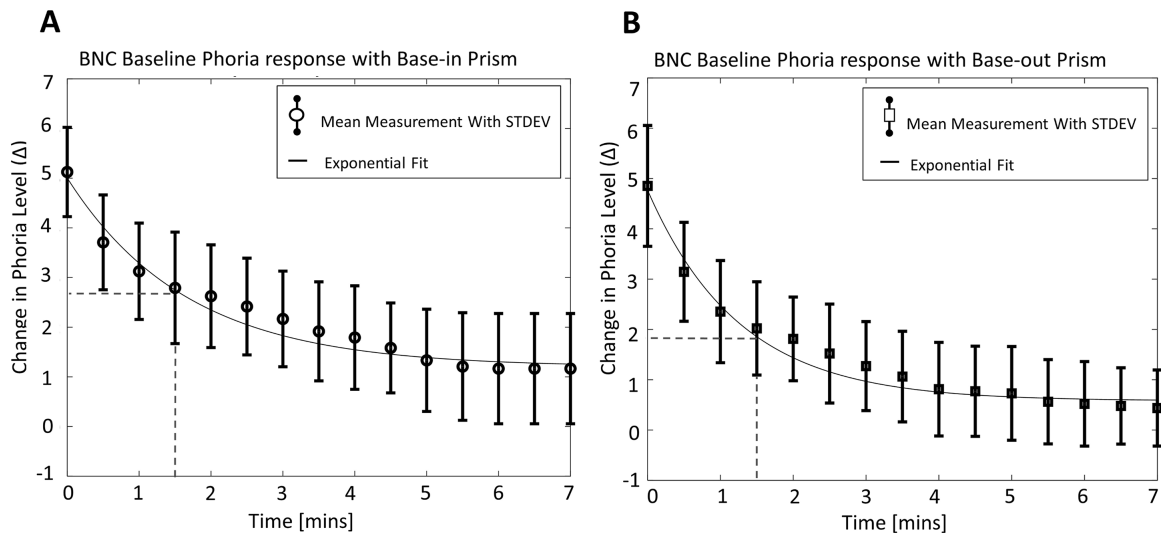
Figure 2. Group-level behavioral phoria adaptation experiment using a 6 base-in prism (A) and 6 base-out prism (B) showing the mean ± *SD* (STDEV) of all participants. The exponential fit of the group is plotted in solid and the dashed line shows the amount of phoria adaptation after 90 seconds, which was the time used within the scanner for sustained fixation.

significant activation level of $p < 0.05$ corrected for multiple comparisons for each visit using cluster-wise FWE described above. Each significantly active voxel was labeled with a binary one and the rest of the voxels as a binary zero. The reliability of spatial extent was assessed using a Boolean AND gate between the two group-level activation maps of the two sessions. The number of surviving voxels within the set of selected ROIs was counted.

Statistical analyses

For all brain activation datasets, a $p < 0.05$ corrected for multiple comparisons was performed with a cluster-wise FWE procedure (Flandin & Friston, 2019). For each visit and each ROI, the mean beta weights and peak beta weights were calculated. To assess test–retest reliability of the mean and peak activation within an ROI, a paired *t*-test was performed within each of the ROIs between visits. A paired *t*-test was performed for each ROI to assess potential significant differences in mean and peak activation between visits. The significance level for all paired *t*-tests was set at $p < 0.05$ false discovery rate corrected for multiple comparisons.

Results

Behavioral phoria adaptation measurements

Because all participants within this study returned to their initial baseline phoria measurement after the 15-minute break, all behavioral phoria adaptation

measurements were completed within a single session early in the day. The mean ± standard deviation (*SD*) values for all participants for the base-out phoria adaptation experiment that stimulated convergence or the near phoria adaptation for the magnitude and rate of the phoria adaptation were $4.3 \pm 1.0\Delta$ and 3.5 ± 1.5 Δ/min, respectively. For the far adaptation assessed using the base-in prism, the mean ± *SD* values for all participants for the magnitude and rate of phoria adaptation were $4.0 \pm 1.2\Delta$ and 2.7 ± 1.4 Δ/min, respectively. Figure 2 shows the group-level phoria adaptation experiment results for the 6 base-in (Figure 2A) and 6 base-out (Figure 2B) group-level data plotting the average phoria level with 1 *SD* as a function of time for the 7-minute experiment. The solid line is the exponential fit of the behavioral data. The dashed line shows the amount of phoria adaptation that occurred at 90 seconds, which is the time used to adapt the phoria within the functional imaging experiment.

Functional activity maps

Figure 3 illustrates the group-level results for 24 of the 29 participants who met the criteria for movement artifacts within the scanner. Five participants were not included in the group-level analysis because the absolute value of movement between time samples was 2 mm or more. The mean ± *SD* for the number of days between scans was 7.3 ± 9 days (range, 1–35 days), which was dependent on the availability of scanner time. Figures 3A and 3B shows the group-level activation maps derived using the delta block from the
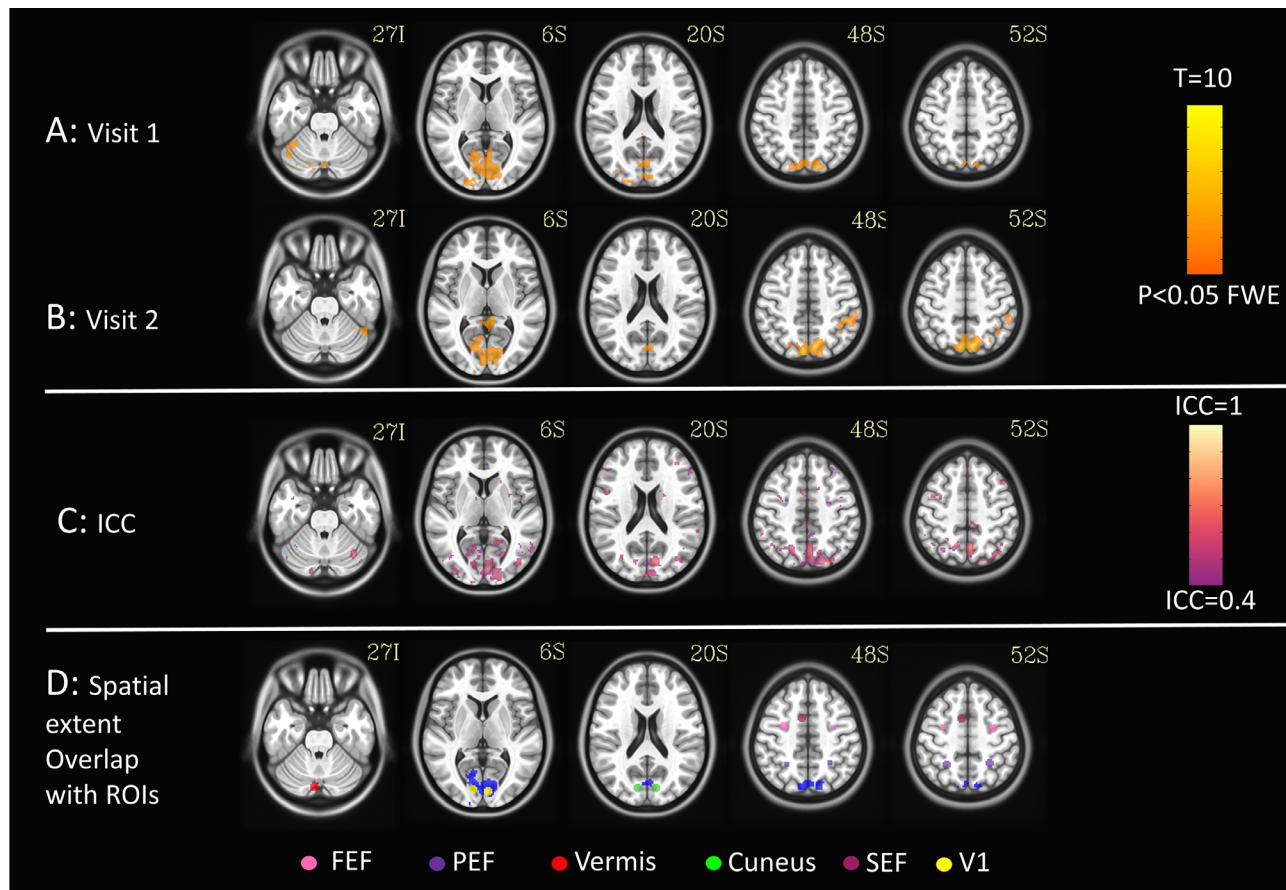
Figure 3. (A) Activation maps for visit 1, and (B) activation maps for visit 2. Oculomotor vermis, V1, and cuneus are significantly active areas. (C) ICC map thresholded at ICC > 0.4, which is fair or better reliability. (D) Spatial extent overlap between visits with selected ROIs. The legend shows the 5-mm sphere for each of the following ROIs: frontal eye fields (FEF) in pink, parietal eye fields (PEF) in purple, vermis in red, cuneus in green, supplemental eye field (SEF) in magenta, and primary visual cortex (V1) in yellow. Slices are designated as I (inferior) or S (superior).

GLM design file for visit 1 and visit 2, respectively. The exponential decay function revealed no significant activation results. A total of five axial slices were presented per visit showing the primary ROIs. The functional activity results were corrected for multiple comparisons using cluster-wise FWE with a significance level threshold fixed at $p < 0.05$ ($t > 3.5$). Significant functional activity was observed within the oculomotor vermis, primary visual cortex, and the left and right cuneus. Supplementary Figures S1 and S2 show additional axial brain slices.

Repeatability

Voxel-wise ICCs

The voxel-wise ICCs were calculated and are shown in Figure 3C. Only ICC values of 0.4 or greater are shown, as depicted by the color scale, because those values fell within the fair, good, or excellent range

(Lukasova et al., 2014). The inferior portion of the oculomotor vermis can be observed within slice 27I. The repeatability of activity for the primary visual cortex is shown in slice 6S, and the cuneus can be observed within the posterior section of slice 20S. For both the primary visual cortex and the cuneus, several voxels reach ICC values from fair to excellent, especially with the right portion of cuneus. The parietal eye fields are located within the bilateral posterior portion shown in slices 48S and 52S, and those ICC values are categorized as fair. The frontal eye fields are bilaterally located within the anterior portion of slices 48S and 52S, where a few voxels have ICC values within the fair range. The supplementary eye field is located within the midline of the prefrontal cortex within slices 48S and 52S, and a few voxels are within fair range. Table 2 lists the peak ICC value for each ROI with the MNI coordinates of the peak ICC value within each ROI. When the peak ICC had been identified, the center of the 5-mm sphere denoting an ROI was optimized to the MNI coordinates of the peak ICC, and the mean ICC

| | | | MNI coordinates (mm) of location for peak ICC | | |
ROIs	Peak ICC within ROIs	Mean ICC within ROIs	x	y	z
Left V1	0.64	0.46	−14	−80	4
Right V1	0.78	0.63	6	−86	4
Left cuneus	0.60	0.46	−14	−78	14
Right cuneus	0.70	0.57	10	−76	18
Left parietal eye field	0.48	0.33	−26	−50	52
Right parietal eye field	0.36	0.31	26	−48	52
Left frontal eye field	0.53	0.40	−32	0	50
Right frontal eye field	0.46	0.29	28	−6	48
Supplementary eye field	0.62	0.50	−6	8	48
Oculomotor vermis	0.28	0.09	−6	−82	−26

Table 2. Intraclass correlation coefficient. Reliability measure is shown within regions of interest. Shown are peak ICC values within selected ROIs and the coordinates of the maximum detected ICC values. Mean ICC was calculated after mean activation within each ROI for visits 1 and 2 independently. Coordinates correspond to the MNI atlas location of the highest ICC value within each ROI.
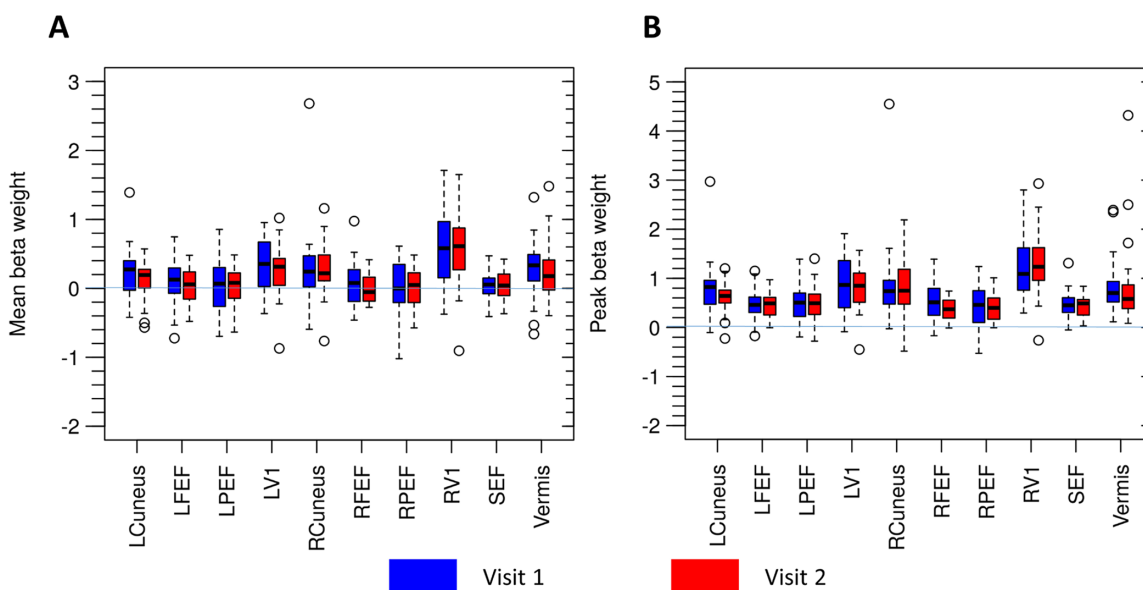

Figure 4. Bar-and-whisker plot for the mean beta weight (4A) and peak beta weight (4B) for the designated ROIs from visit 1 (blue) and visit 2 (red).

for each ROI was calculated using the mean activation within each ROI per participant (Table 2).

Figure 3D shows the repeatability of spatial extent between visits 1 and 2 and plots the functional activity observed from the group datasets during both visits. The legend shows the different ROIs in different colors, where each ROI is a 5-mm sphere centered around the peak ICC value tabulated in Table 2. The total number of surviving voxels in the map of repeatability of spatial extent for each of the following ROIs were 75 voxels within the primary right visual cortex, 16 voxels within the left primary visual cortex, 5 voxels within the right cuneus, 3 voxels within the left cuneus, and 3 voxels within the cerebellar vermis.

Consistency of beta weights between visits 1 and 2

Figure 4 shows the mean beta weight results for each ROI with box-and-whisker plots (Figure 4A) and the peak beta weights for each ROI (Figure 4B) for visit 1 (blue box) and visit 2 (red box). Outliers are shown as black circles in the same vertical axis of the box. The one-sample t-test showed significant activation with the GLM for the mean beta values for the following: left primary visual cortex during visit 1, $T(23) = 3.91$, and visit 2, $T(23) = 3.14$; right primary visual cortex during visit 1, $T(23) = 4.8$, and visit 2, $T(23) = 5.46$; left cuneus during visit

1, $T(23) = 2.55$, but not visit 2, $T(23) = 1.9$; right cuneus during visit 1, $T(23) = 2.40$, and visit 2, $T(23) = 3.43$; and oculomotor vermis during visit 1, $T(23) = 3.24$, and visit 2, $T(23) = 2.84$ ($p < 0.05$ corrected for multiple comparison with false discovery rate). No other brain regions showed significant activity.

Discussion

In this study of young adult participants with normal binocular vision, using a novel phoria adaptation paradigm, the results support the suggestion that the primary neural substrates activated within a phoria adaptation task are the oculomotor vermis and bilateral cuneus. Furthermore, the repeatability, also called the test–retest reliability of the testing protocol used, was fair for the oculomotor vermis and good for the cuneus using predetermined criterion established within the literature. This is important because this protocol can now be used as an outcome measure within future randomized clinical trials to investigate differences between control participants with normal binocular vision and those with binocular dysfunction, as well as to assess the underlying mechanism of various therapeutic interventions.

Oculomotor vermis

Significant and repeatable functional activity was observed within the oculomotor vermis, specifically the vermal VI and VII regions. Electrophysiology studies on three rhesus macaque primates support the idea that, when the dorsal portion of the cerebellar vermis is lesioned, the ability to perform phoria adaptation is substantially diminished (Takagi et al., 2003). Patients with cerebellar vermis dysfunction and deficits are reported to have a decrease in phoria adaptation (Kono, Hasebe, Ohtsuki, Kashihara, & Shiro, 2002; Milder & Reinecke, 1983). To the best of our knowledge, this study is the first to conduct a detailed study on phoria adaptation using functional imaging on binocularly normal control participants. One prior functional imaging study on control participants studied the impact of prism adaptation on the accuracy of finger pointing and reported significant activation in the cerebellar vermis region (Küper et al., 2014). Based on electrophysiology studies on primates, patients with cerebellar deficits, and a functional imagining study on finger pointing accuracy when viewed through a prism, several modalities of research support the concept that the cerebellar vermis is a neural substrate involved in the process of phoria adaptation.

Cuneus

Although not part of the initial hypothesis, the functional imaging results of the present study revealed significant and repeatable activity within the bilateral cuneus. Functional imaging studies using sustained visual attention tasks such as the symbol digit modality test (da Silva, Secchinato, Rondinoni, & Leoni, 2020) and visual search testing (Parker, Zalusky, & Kirbas, 2014) support the idea that the cuneus is functionally active during sustained visual attention. Prior magnetoencephalography studies on humans revealed that the cuneus is responsible for sustained visual attention (Vanni, Tanskanen, Seppä, Uutela, & Hari, 2001). Several studies also support the suggestion that the cuneus is functionally active for the spatial awareness of the location of objects (Goodale & Milner, 1992; Laycock, Cross, Lourenco, & Crewther, 2011; Noguchi, Inui, & Kakigi, 2004). Together, these results suggest that phoria adaptation, which is a sustained visual attention task, does recruit the bilateral cuneus to modify the phoria adaptation system.

Visual cortex

The visual cortex was functionally active during the visual task presented here that alternated between near crossed and far uncrossed binocular stimulation. In studies comparing binocularly normal controls to patients with amblyopia, significant differences were observed between the groups, such that ambylopes had disturbances for the integration of binocular signals within the visual cortex (Jurcoane, Choubey, Mitsieva, Muckli, & Sireteanu, 2009; Jurcoane, Choubey, Muckli, & Sireteanu, 2007). An extensive review summarizes the culmination of electrophysiology studies on animals and functional imaging on humans and suggests that binocular disparity is processed within the visual cortex (Joly & Frankó, 2014). In summary, these studies support the theory that the process of stereopsis does occur within the visual cortex and hence could explain the stimulus activation observed within the visual cortex from our results.

Frontoparietal network

The visual task of sustained near crossed and far uncrossed fixation stimulated functional activity within the parietal, frontal, and supplementary eye fields. All of these regions have been reported to be active during vergence eye movements in humans using functional imaging (Alvarez et al., 2010; Jaswal et al., 2014; Morales et al., 2020). The frontal, parietal, and supplementary eye fields are also stimulated

during visual attention tasks specifically within the frontoparietal network from electrophysiology studies of primates (da Silva et al., 2020; Thiele, Brandt, Dasilva, Gotthardt, Chicharro, Panzeri, & Distler, 2016; Wardak, Olivier, & Duhamel, 2011) and functional imaging on humans (Beauchamp, Petit, Ellmore, Ingeholm, & Haxby, 2001; Meehan, Bressler, Tang, Astafiev, Sylvester, Shulman, & Corbetta, 2017; Meyer, Du, Parks, & Hopfinger, 2018). The frontal eye fields have also been reported to be modulated for disparity signals (da Silva et al., 2020; Ferraina, Pare, & Wurtz, 2000; Gamlin & Yoon, 2000; Genovesio & Ferraina, 2004; Nunes, Monteiro, Ferreira, & Nunes, 2019). Collectively, prior research from electrophysiology and functional imaging studies support the suggestion that visual attention that is utilized within a phoria adaptation experiment stimulates the frontoparietal networks.

Clinical relevance

Previous clinical studies have demonstrated that phoria adaptation is reduced in patients with binocular dysfunction such as convergence insufficiency (Brautaset & Jennings, 2005a; Brautaset & Jennings, 2006; Henson & North, 1980; North & Henson, 1981; Schor & Horner, 1989; Sreenivasan & Bobier, 2014), exotropia (Kiyak Yilmaz, Kose, Yilmaz, & Uretmen, 2015; Zahavi, Friling, Ron, Ehrenberg, Nahum, & Snir, 2019), convergence excess esotropia (Garretty, 2018; Wygnanski-Jaffe, Trotter, Watts, Kraft, & Abdolell, 2003), and decompensated heterophoria (Przekoracka-Krawczyk, Michalak, & Pyżalska, 2019). In addition, there is evidence that therapeutic interventions such as vision therapy (Brautaset & Jennings, 2006) or surgery (Akbari, Mehrabi Bahar, Mirmohammadsadeghi, Bayat, & Masoumi, 2018; Garretty, 2018) may lead to an improvement in phoria adaptation in some patients. Thus, both the assessment and treatment of phoria adaptation are important in the care of patients with binocular dysfunction. The results of this study using fMRI testing are important because they establish the underlying neural substrates that mediate phoria adaptation. Because this testing revealed significant functional activity within the brain and the results were repeatable, this measurement could be a valuable addition to future randomized clinical trials studying the treatment of patients with binocular dysfunction.

Study limitations and future directions

Although group-level analyses showed good repeatability from visit 1 to visit 2 for the primary ROIs, the spatial extent was not as consistent as the mean and peak beta weight within these ROIs. For this reason, caution should be exercised if spatial extent is to be used as an outcome measurement. The eye tracking during the scanning session was monocular. We can confirm that all participants did perform the task, but we cannot report the vergence angle during the scans, which is a study limitation. In addition, the optimal amount of time for phoria adaptation within the scanner is challenging to determine. A compromise must be found between limiting head motion by not having an experimental task be too long and allowing as much time as possible for the phoria adaptation. Because our results have good repeatability, we did stimulate phoria adaptation to provoke consistent functional activity while not having excessive head motion.

Future studies should investigate the difference in phoria adaptation in clinical populations with binocular dysfunctions compared to participants with normal binocular vision using fMRI as an outcome measure. In addition, this fMRI protocol could be a valuable outcome measure in future randomized clinical trials to assess therapeutic interventions for patients with binocular vision.

Conclusion

This study establishes the neural substrates activated within a phoria adaptation task, and masks have been established to define ROIs within young adult participants with normal binocular vision. The experimental method and image processing described for phoria adaptation indicate that this protocol is repeatable within the oculomotor vermis and cuneus. Hence, the described protocol and analysis on phoria adaptation may be used as a potential outcome measure in future randomized clinical trials.

Keywords: functional MRI, phoria adaptation, reliability, intraclass correlation coefficient, oculomotor vermis, cuneus, binocular dysfunction

Acknowledgments

Commercial relationships: none.
Corresponding author: Tara L. Alvarez.
Email: tara.l.alvarez@njit.edu.
Address: Department of Biomedical Engineering, New Jersey Institute of Technology, Newark, NJ, USA.

References

Akbari, M. R., Mehrabi Bahar, M. R., Mirmohammadsadeghi, A., Bayat, R., & Masoumi, A. (2018). Short prism adaptation test in patients with acquired nonaccommodative esotropia; clinical findings and surgical outcome. *Journal of AAPOS, 22*(5), 352–355.

Alvarez, T. L., Alkan, Y., Gohel, S., Ward, B. D., & Biswal, B. B. (2010). Functional anatomy of predictive vergence and saccade eye movements in humans: A functional MRI investigation. *Vision Research, 50*(21), 2163–2175.

Alvarez, T. L., Jaswal, R., Gohel, S., & Biswal, B. B. (2014). Functional activity within the frontal eye fields, posterior parietal cortex, and cerebellar vermis significantly correlates to symmetrical vergence peak velocity: An ROI-based, fMRI study of vergence training. *Frontiers in Integrative Neuroscience, 8*, 50.

Alvarez, T. L., Kim, E. H., & Granger-Donetti, B. (2017). Adaptation to progressive additive lenses: Potential factors to consider. *Scientific Reports, 7*(1), 2529.

Alvarez, T. L., Scheiman, M., Santos, E. M., Morales, C., Yaramothu, C., D'Antonio-Bertagnolli, J. V., … Li, X. (2020). The Convergence Insufficiency Neuro-mechanism in Adult Population Study (CINAPS) randomized clinical trial: Design, methods, and clinical data. *Ophthalmic Epidemiology, 27*(1), 52–72.

Alvarez, T. L., Vicci, V. R., Alkan, Y., Kim, E. H., Gohel, S., Barrett, A. M., … Biswal, B. B. (2010). Vision therapy in adults with convergence insufficiency: Clinical and functional magnetic resonance imaging measures. *Optometry and Vision Science, 87*(12), E985–E1002.

Beauchamp, M. S., Petit, L., Ellmore, T. M., Ingeholm, J., & Haxby, J. V. (2001). A parametric fMRI study of overt and covert shifts of visuospatial attention. *NeuroImage, 14*(2), 310–321.

Behzadi, Y., Restom, K., Liau, J., & Liu, T. T. (2007). A component based noise correction method (CompCor) for BOLD and perfusion based fMRI. *NeuroImage, 37*(1), 90–101.

Borsting, E. J., Rouse, M. W., Mitchell, G. L., Scheiman, M., Cotter, S. A., & Cooper, J., …, Convergence Insufficiency Treatment Trial Group. (2003). Validity and reliability of the revised convergence insufficiency symptom survey in children aged 9 to 18 years. *Optometry and Vision Science, 80*(12), 832–838.

Bostan, A. C., & Strick, P. L. (2018). The basal ganglia and the cerebellum: Nodes in an integrated network. *Nature Reviews Neuroscience, 19*(6), 338–350.

Brainard, D. H. (1997). The Psychophysics Toolbox. *Spatial Vision, 10*(4), 433–436.

Brautaset, R L, & Jennings, J. A. M. (2005a). Distance vergence adaptation is abnormal in subjects with convergence insufficiency. *Ophthalmic and Physiological Optics, 25*(3), 211–214.

Brautaset, R. L., & Jennings, J. A. M. (2005b). Horizontal and vertical prism adaptation are different mechanisms. *Ophthalmic and Physiological Optics, 25*(3), 215–218.

Brautaset, R. L., & Jennings, A. J. M. (2006). Effects of orthoptic treatment on the CA/C and AC/A ratios in convergence insufficiency. *Investigative Ophthalmology & Visual Science, 47*(7), 2876–2880, https://doi.org/10.1167.

Brett, M., Anton, J. L., Valabregue, R., & Poline, J. B. (2002). Region of interest analysis using an SPM toolbox. In *Proceedings of the 8th International Conference on Functional Mapping of the Human Brain* (p. 497), Cambridge, MA: Academic Press.

Bucci, M. P., Brémond-Gignac, D., & Kapoula, Z. (2008). Poor binocular coordination of saccades in dyslexic children. *Graefe's Archive for Clinical and Experimental Ophthalmology, 246*(3), 417–428.

Bucci, M. P., Nassibi, N., Gérard, C.-L., Bui-Quoc, E., & Seassau, M. (2012). Immaturity of the oculomotor saccade and vergence interaction in dyslexic children: Evidence from a reading and visual search study. *PLoS One, 7*(3), e33458.

Chen, Y. F., Lee, Y. Y., Chen, T., Semmlow, J. L., & Alvarez, T. L. (2010). Review: Behaviors, models, and clinical applications of vergence eye movements. *Journal of Medical and Biological Engineering, 30*(1), 1–15.

CITT-ART Investigator Group, Scheiman, M., Mitchell, G. L, Cotter, S. A, Kulp, M, Chase, C., & Hertle, R. (2015). Convergence Insufficiency Treatment Trial - Attention and Reading Trial (CITT-ART): Design and methods. *Vision Development and Rehabilitation, 1*(3), 214–228.

da Silva, P. H. R., Secchinato, K. F., Rondinoni, C., & Leoni, R. F. (2020). Brain structural-functional connectivity relationship underlying the information processing speed. *Brain Connectivity, 10*(3), 143–154.

Eckert, M. A., Leonard, C. M., Richards, T. L., Aylward, E. H., Thomson, J., & Berninger, V. W. (2003). Anatomical correlates of dyslexia: Frontal and cerebellar findings. *Brain, 126*(2), 482–494.

Ferraina, S., Pare, M., & Wurtz, R. H. (2000). Disparity sensitivity of frontal eye field neurons. *Journal of Neurophysiology, 83*(1), 625–629.

Flandin, G., & Friston, K. J. (2019). Analysis of family-wise error rates in statistical parametric mapping using random field theory. *Human Brain Mapping, 40*(7), 2052–2054.

Friston, K. J., Williams, S., Howard, R., Frackowiak, R. S., & Turner, R. (1996). Movement-related effects in fMRI time-series. *Magnetic Resonance in Medicine, 35*(3), 346–355.

Gaertner, C., Creux, C., Espinasse-Berrod, M. A., Orssaud, C., Dufier, J. L., & Kapoula, Z. (2013). Postural control in nonamblyopic children with early-onset strabismus. *Investigative Ophthalmology & Visual Science, 54*(1), 529–536, https://doi.org/10.1167/iovs.12-10586.

Gamlin, P. D. R., & Yoon, K. (2000). An area for vergence eye movement in primate frontal cortex. *Nature, 407*(6807), 1003–1007.

Garretty, T. (2018). The effect of prism adaptation on the angle of deviation in convergence excess esotropia and possible consequences for surgical planning. *Strabismus, 26*(3), 111–117.

Genovesio, A., & Ferraina, S. (2004). Integration of retinal disparity and fixation-distance related signals toward an egocentric coding of distance in the posterior parietal cortex of primates. *Journal of Neurophysiology, 91*(6), 2670–2684.

Goodale, M. A., & Milner, A. D. (1992). Separate visual pathways for perception and action. *Trends in Neurosciences, 15*(1), 20–25.

Gorgolewski, K. J., Storkey, A. J., Bastin, M. E., Whittle, I., & Pernet, C. (2013). Single subject fMRI test-retest reliability metrics and confounding factors. *NeuroImage, 69*, 231–243.

Guo, Y. Y., Kim, E. H., & Alvarez, T. L. (2011). VisualEyes: A modular software system for oculomotor experimentation. *Journal of Visualized Experiments, (49)*, 2530.

Han, S. J., Guo, Y., Granger-Donetti, B., Vicci, V. R., & Alvarez, T. L. (2010). Quantification of heterophoria and phoria adaptation using an automated objective system compared to clinical methods. *Ophthalmic and Physiological Optics, 30*(1), 95–107.

Henson, D. B., & North, R. (1980). Adaptation to prism-induced heterophoria. *American Journal of Optometry and Physiological Optics, 57*(3), 129–137.

Jaswal, R., Gohel, S., Biswal, B. B., & Alvarez, T. L. (2014). Task-modulated coactivation of vergence neural substrates. *Brain Connectivity, 4*(8), 595–607.

Jiang, B.-C., Tea, Y. C., & O'Donnell, D. (2007). Changes in accommodative and vergence responses when viewing through near addition lenses. *Optometry, 78*(3), 129–134.

Joly, O., & Frankó, E. (2014). Neuroimaging of amblyopia and binocular vision: A review. *Frontiers in Integrative Neuroscience. 8*, 62.

Judge, S. J. (1996). How is binocularity maintained during convergence and divergence? *Eye, 10*(2), 172–176.

Jurcoane, A., Choubey, B., Mitsieva, D., Muckli, L., & Sireteanu, R. (2009). Interocular transfer of orientation-specific fMRI adaptation reveals amblyopia-related deficits in humans. *Vision Research, 49*(13), 1681–1692.

Jurcoane, A., Choubey, B., Muckli, L., & Sireteanu, R. (2007). A pilot study for investigating cortical binocularity in humans using fMRI adaptation. *Strabismus, 15*(1), 33–37.

Kapoula, Z., & Bucci, M. P. (2007). Postural control in dyslexic and non-dyslexic children. *Journal of Neurology, 254*(9), 1174–1183.

Kim, E. H., Granger-Donetti, B., Vicci, V. R., & Alvarez, T. L. (2010). The relationship between phoria and the ratio of convergence peak velocity to divergence peak velocity. *Investigative Ophthalmology & Visual Science, 51*(8), 4017–4027, https://doi.org/10.1167/iovs.09-4560.

Kim, E. H., Vicci, V. R., Granger-Donetti, B., & Alvarez, T. L. (2011). Short-term adaptations of the dynamic disparity vergence and phoria systems. *Experimental Brain Research, 212*(2), 267–278.

Kim, E. H., Vicci, V. R., Han, S. J., & Alvarez, T. L. (2011). Sustained fixation induced changes in phoria and convergence peak velocity. *PLoS One, 6*(6), e20883.

Kiyak Yilmaz, A., Kose, A. S., Yilmaz, G. S., & Uretmen, O. (2015). The impact of prism adaptation test on surgical outcomes in patients with primary exotropia. *Clinical & Experimental Optometry, 98*(3), 224–227.

Kono, R., Hasebe, S., Ohtsuki, H., Kashihara, K., & Shiro, Y. (2002). Impaired vertical phoria adaptation in patients with cerebellar dysfunction. *Investigative Ophthalmology & Visual Science, 43*(3), 673–678.

Küper, M., Wünnemann, M. J. S., Thürling, M., Stefanescu, R. M., Maderwald, S., Elles, H. G., . . . Timmann, D. (2014). Activation of the cerebellar cortex and the dentate nucleus in a prism adaptation fMRI study. *Human Brain Mapping, 35*(4), 1574–1586.

Laycock, R., Cross, A. J., Lourenco, T., & Crewther, S. G. (2011). Dorsal stream involvement in recognition of objects with transient onset but not with ramped onset. *Behavioral and Brain Functions, 7*, 34.

Lee, Y. Y., Granger-Donetti, B., Chang, C., & Alvarez, T. L. (2009). Sustained convergence induced

changes in phoria and divergence dynamics. *Vision Research, 49*(24), 2960–2972.

Legrand, A., Bui-Quoc, E., Doré-Mazars, K., Lemoine, C., Gérard, C. L., & Bucci, M. P. (2012). Effect of a dual task on postural control in dyslexic children. *PLoS One, 7*(4), e35301.

Li, L., Zeng, L., Lin, Z., Cazzell, M., & Liu, H. (2015). Tutorial on use of intraclass correlation coefficients for assessing intertest reliability and its application in functional near-infrared spectroscopy-based brain imaging. *Journal of Biomedical Optics, 20*(5), 050801.

Lukasova, K., Sommer, J., Nucci-da-silva, M. P., Vieira, G., Blanke, M., Bremmer, F., . . . Bremmer, F. (2014). Test-retest reliability of fMRI activation generated by different saccade tasks. *Journal of Magnetic Resonance Imaging, 40*(1), 37–46.

Meehan, T. P., Bressler, S. L., Tang, W., Astafiev, S. V., Sylvester, C. M., Shulman, G. L., . . . Corbetta, M. (2017). Top-down cortical interactions in visuospatial attention. *Brain Structure and Function, 222*(7), 3127–3145.

Meyer, K. N., Du, F., Parks, E., & Hopfinger, J. B. (2018). Exogenous vs. endogenous attention: Shifting the balance of fronto-parietal activity. *Neuropsychologia, 111*, 307–316.

Milder, D. G., & Reinecke, R. D. (1983). Phoria adaptation to prisms: A cerebellar-dependent response. *Archives of Neurology, 40*(6), 339–342.

Molinari, M., Leggio, M. G., Solida, A., Ciorra, R., Misciagna, S., Silveri, M. C., . . . Petrosini, L. (1997). Cerebellum and procedural learning: Evidence from focal cerebellar lesions. *Brain, 120*, 1753–1762.

Monti, M. (2011). Statistical analysis of fMRI time-series: A critical review of the GLM approach. *Frontiers in Human Neuroscience, 5*, 28.

Morales, C., Gohel, S., Li, X., Scheiman, M., Biswal, B. B., Santos, E. M., . . . Alvarez, T. L. (2020). Test-retest reliability of functional magnetic resonance imaging activation for a vergence eye movement task. *Neuroscience Bulletin, 36*(5), 506–518.

Morrison, M. A., Das, S., Graham, S. J., Cusimano, M. D., Schweizer, T. A., & Churchill, N. W. (2016). Reliability of task-based fMRI for preoperative planning: A test-retest study in brain tumor patients and healthy controls. *PLoS One, 11*(2), e0149547.

Nicolson, R. I., Fawcett, A. J., & Dean, P. (2001). Developmental dyslexia: The cerebellar deficit hypothesis. *Trends in Neurosciences*, *24*(9), 508–511.

Noguchi, Y., Inui, K., & Kakigi, R. (2004). Temporal dynamics of neural adaptation effect in the human visual ventral stream. *Journal of Neuroscience, 24*(28), 6283–6290.

North, R., & Henson, D. B. (1981). Adaptation to prism-induced heterophoria in subjects with abnormal binocular vision or asthenopia. *American Journal of Optometry and Physiological Optics, 58*(9), 746–752.

Nunes, A. F., Monteiro, P. M. L., Ferreira, F. B. P., & Nunes, A. S. (2019). Convergence insufficiency and accommodative insufficiency in children. *BMC Ophthalmology, 19*(1), 58.

Parker, J. G., Zalusky, E. J., & Kirbas, C. (2014). Functional MRI mapping of visual function and selective attention for performance assessment and presurgical planning using conjunctive visual search. *Brain and Behavior, 4*(2), 227–237.

Przekoracka-Krawczyk, A., Brenk-Krakowska, A., Nawrot, P., Rusiak, P., & Naskręcki, R. (2017). Unstable binocular fixation affects reaction times but not implicit motor learning in dyslexia. *Investigative Ophthalmology & Visual Science, 58*(14), 6470–6480, https://doi.org/10.1167/iovs.16-21305.

Przekoracka-Krawczyk, A., Michalak, K. P., & Pyżalska, P. (2019). Deficient vergence prism adaptation in subjects with decompensated heterophoria. *PLoS One, 14*(1), e0211039.

Przekoracka-Krawczyk, A., Nawrot, P., Kopyciuk, T., & Naskręcki, R. (2015). Implicit motor learning is impaired in strabismic adults. *Journal of Vision, 15*(11), 1–20, https://doi.org/10.1167/15.11.6.

Raymond, J. L., & Medina, J. F. (2018). Computational principles of supervised learning in the cerebellum. *Annual Review of Neuroscience, 41*(1), 233–253.

Robertson, E. M., & Miall, R. C. (1999). Visuomotor adaptation during inactivation of the dentate nucleus. *NeuroReport, 10*(5), 1029–1034.

Santos, E. M., Yaramothu, C., & Alvarez, T. L. (2018). Comparison of symmetrical prism adaptation to asymmetrical prism adaptation in those with normal binocular vision. *Vision Research, 149*, 59–65.

Scheiman, M., & Wick, B. (2020). *Clinical management of binocular vision: Heterophoric, accommodative, and eye movement disorders* (5th ed.). Philadelphia, PA: Lippincott Williams & Wilkins.

Schor, C. M. (1988). Influence of accommodative and vergence adaptation on binocular motor disorders. *American Journal of Optometry and Physiological Optics, 65*(6), 464–475.

Schor, C. M., & Horner, D. (1989). Adaptive disorders of accommodation and vergence in binocular dysfunction. *Ophthalmic & Physiological Optics, 9*(3), 264–268.

Servatius, R. J., Spiegler, K. M., Handy, J. D., Pang, K. C. H., Tsao, J. W., & Mazzola, C. A. (2018). Neurocognitive and fine motor deficits in asymptomatic adolescents during the subacute period after concussion. *Journal of Neurotrauma, 35*(8), 1008–1014.

Shrout, P. E., & Fleiss, J. L. (1979). Intraclass correlations: Uses in assessing rater reliability. *Psychological Bulletin*, *86*(2), 420–428.

Sreenivasan, V., & Bobier, W. R. (2014). Reduced vergence adaptation is associated with a prolonged output of convergence accommodation in convergence insufficiency. *Vision Research, 100*, 99–104.

Sreenivasan, V., Irving, E. L., & Bobier, W. R. (2008). Binocular adaptation to near addition lenses in emmetropic adults. *Vision Research, 48*(10), 1262–1269.

Sreenivasan, V., Irving, E. L., & Bobier, W. R. (2009). Binocular adaptation to +2 D lenses in myopic and emmetropic children. *Optometry and Vision Science, 86*(6), 731–740.

Stoodley, C. J., Fawcett, A. J., Nicolson, R. I., & Stein, J. F. (2005). Impaired balancing ability in dyslexic children. *Experimental Brain Research, 167*(3), 370–380.

Takagi, M., Tamargo, R., & Zee, D. S. (2003). Effects of lesions of the cerebellar oculomotor vermis on eye movements in primate: Binocular control. *Progress in Brain Research, 142*, 19–33.

Thiele, A., Brandt, C., Dasilva, M., Gotthardt, S., Chicharro, D., Panzeri, S., . . . Distler, C. (2016). Attention induced gain stabilization in broad and narrow-spiking cells in the frontal eye-field of macaque monkeys. *Journal of Neuroscience, 36*(29), 7601–7612.

Vanni, S., Tanskanen, T., Seppä, M., Uutela, K., & Hari, R. (2001). Coinciding early activation of the human primary visual cortex and anteromedial cuneus. *Proceedings of the National Academy of Sciences, USA, 98*(5), 2776–2780.

Vicari, S., Finzi, A., Menghini, D., Marotta, L., Baldi, S., & Petrosini, L. (2005). Do children with developmental dyslexia have an implicit learning deficit? *Journal of Neurology, Neurosurgery and Psychiatry, 76*(10), 1392–1397.

Vicari, S., Marotta, L., Menghini, D., Molinari, M., & Petrosini, L. (2003). Implicit learning deficit in children with developmental dyslexia. *Neuropsychologia, 41*(1), 108–114.

Wardak, C., Olivier, E., & Duhamel, J. R. (2011). The relationship between spatial attention and saccades in the frontoparietal network of the monkey. *European Journal of Neuroscience, 33*(11), 1973–1981.

Wygnanski-Jaffe, T., Trotter, J., Watts, P, Kraft, F.P., & Abdolell, M. (2003). Preoperative prism adaptation in acquired esotropia with convergence excess. *Journal of American Association for Pediatric Ophthalmology and Strabismus, 7*(1), 28–33.

Yan, C.-G., Cheung, B., Kelly, C., Colcombe, S., Craddock, R. C., Martino, A., . . . Milham, M. P. (2013). A comprehensive assessment of regional variation in the impact of head micromovements on functional connectomics. *NeuroImage, 76*, 183–201.

Zahavi, A., Friling, R., Ron, Y., Ehrenberg, M., Nahum, Y., & Snir, M. (2019). Evaluation of ocular motility deviation changes in exotropic patients after cycloplegic eye drops versus prism adaptation test. *European Journal of Ophthalmology, 29*(5), 482–485.

Zuo, X., Di, A., Kelly, C., Shehzad, Z. E., Gee, D. G., Klein, D. F., . . . Milham, M. P. (2010). The oscillating brain: Complex and reliable. *NeuroImage, 49*(2), 1432–1445.

Zuo, X., Kelly, C., Adelstein, J. S., Klein, D. F., Castellanos, F. X., & Milham, M. P. (2010). Reliable intrinsic connectivity networks: Test-retest evaluation using ICA and dual regression approach. *NeuroImage, 49*(3), 2163–2177.